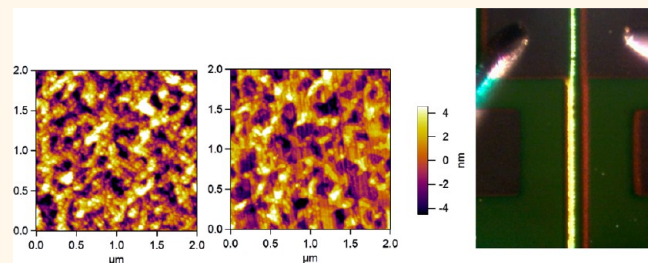


# Ordered Polymer Nanofibers Enhance Output Brightness in Bilayer Light-Emitting Field-Effect Transistors

Ben B.Y. Hsu,<sup>†</sup> Jason Seifter,<sup>†</sup> Christopher J. Takacs,<sup>†</sup> Chengmei Zhong,<sup>†</sup> Hsin-Rong Tseng,<sup>†</sup> Ifor D. W. Samuel,<sup>‡</sup> Ebinaazar B. Namdas,<sup>§</sup> Guillermo C. Bazan,<sup>†</sup> Fei, Huang,<sup>†</sup> Yong Cao,<sup>†</sup> and Alan J. Heeger<sup>†,\*</sup>

<sup>†</sup>Center for Polymers and Organic Solids, University of California, Santa Barbara, United States, <sup>‡</sup>Organic Semiconductor Centre, SUPA, School of Physics and Astronomy, University of St Andrews, U.K., <sup>§</sup>Centre for Organic Photonics and Electronics, The University of Queensland, Australia 4072, and <sup>†</sup>Institute of Polymer Optoelectronic Materials & Devices, State Key Laboratory of Luminescent Materials and Devices, South China University of Technology, P.R. China

**ABSTRACT** Polymer light emitting field effect transistors are a class of light emitting devices that reveal interesting device physics. Device performance can be directly correlated to the most fundamental polymer science. Control over surface properties of the transistor dielectric can dramatically change the polymer morphology, introducing ordered phase. Electronic properties such as carrier mobility and injection efficiency on the interface can be promoted by ordered nanofibers in the polymer. Moreover, by controlling space charge in the polymer interface, the recombination zone can be spatially extended and thereby enhance the optical output.



**KEYWORDS:** organic semiconductors · light emitting field effect transistor · bilayer · ordering · oriented polymer

Current density and recombination efficiency are the most critical parameters for achieving high performance organic light emitting devices. Organic light emitting diodes (OLEDs) show outstanding brightness because high current density is injected into a well-designed multilayer structure. For flat panel displays, however, the high current density must be driven by high mobility transistors made by complex (and expensive) photolithography.

Light emitting field-effect transistors (LEFETs) combine the advantages of light emitting diodes and field-effect transistors (FETs). LEFETs provide promising brightness<sup>1–3</sup> and efficiency<sup>4–8</sup> and can be made by using relatively simple fabrication processes. Though LEFETs offer significant benefits, they currently suffer from low carrier mobility in the FET transport channel, resulting in low current density for light emission. Moreover, because hole transport is dominant in most semiconducting polymers, the recombination efficiency is limited. The unbalanced transport can in principle be solved by utilizing ambipolar light emitting polymers. However, their mobilities are relatively low

(typically  $10^{-3}$  to  $0.11\text{ cm}^2/(\text{V s})$ ), and there are relatively few candidate materials.<sup>9–13</sup> The light intensities obtained from red–green–blue (RGB) LEFETs are limited. Therefore, a device architecture that can universally offer basic RGB colors with high brightness would represent important progress.

Although different device geometries and molecules have been surveyed,<sup>14–26</sup> only the bilayer architecture has demonstrated RGB emission<sup>27</sup> with promising brightness. The device architecture is shown in Figure 1 along with the molecular structures of the hole-transporting polymer poly(3,6-di-alkylthieno[3,2-b]thiophene-co-bithiophene) (PATBT), the light emitting polymer Super Yellow (SY), and the interlayer comprising the hole blocking/electron injecting conjugated polymer electrolyte (CPE). A photo showing the operating LEFET is also included in Figure 1.

In the bilayer LEFET, we expect that improved order of the polymer in the hole-transport layer should improve the mobility (current density) and hence increase the overall brightness. Ordered morphologies

\* Address correspondence to ajhe1@physics.ucsb.edu.

Received for review December 1, 2012 and accepted February 15, 2013.

Published online February 15, 2013  
10.1021/nn305566u

© 2013 American Chemical Society

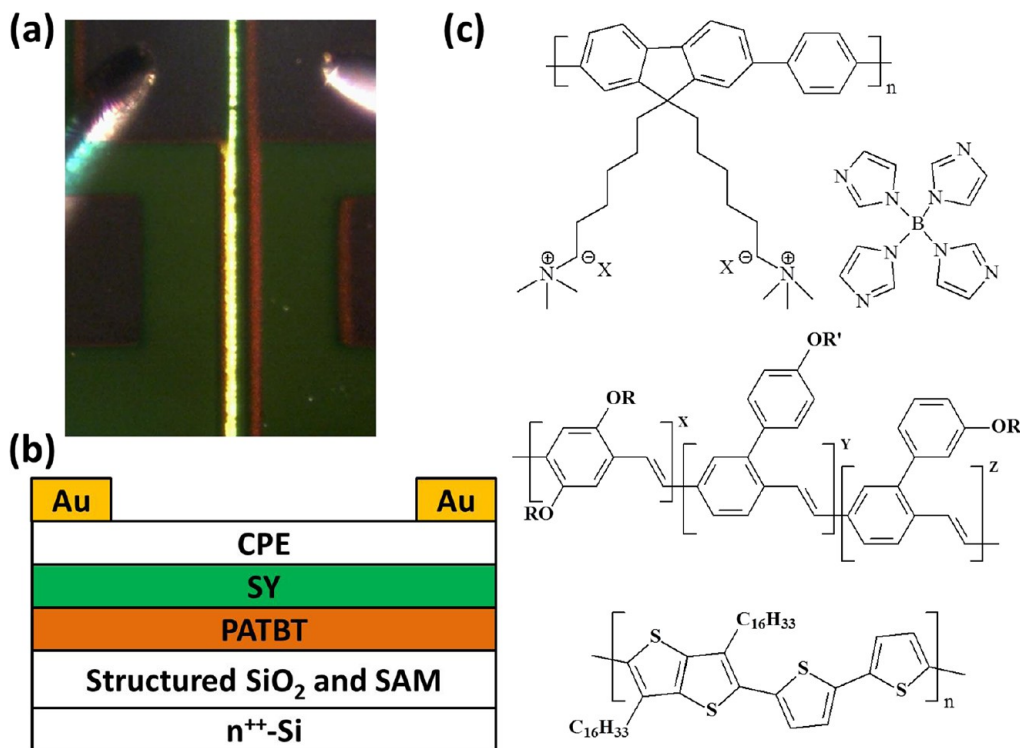


Figure 1. (a) Photo of the operating device; (b) schematic of the device architecture; (c) molecular structures of PFN<sup>+</sup>Blm<sub>4</sub><sup>-</sup> CPE, Super Yellow, and PATBT.

can be achieved by various methods, the enhancement from reported works such as e-beam lithography, contact imprinting, electrospinning,<sup>31–36</sup> and flow coating<sup>37</sup> was interpreted in terms of morphology,<sup>37</sup> optical properties,<sup>32–35</sup> and short-term order<sup>36</sup> instead of electronic mobility enhanced by long-term order.<sup>38–40</sup> Moreover, e-beam lithography and contact printing are both demanding on expertise and facilities.

We demonstrate that the brightness can be increased from about 2000 cd/m<sup>2</sup> to over 9000 cd/m<sup>2</sup> by improving the hole-mobility from 0.03 to >0.5 cm<sup>2</sup>/(V s) through the use of a nanostructured SiO<sub>2</sub> dielectric interface. The nanostructured interface is formed by directional rubbing of the gate dielectric with diamond lapping film, forming few-to-tens angstrom deep and few-to-tens nanometer wide grooves that extend from hundreds-of-nanometers to micrometers in length with nearly arbitrary density. For the polymer PATBT, we find that the mobility is anisotropic in spin-cast films and is improved in the direction parallel to the scratches as compared to the flat substrates.

In these highly unbalanced transport conditions, space charge effects would be expected to play an important role in both electronic and optoelectronic aspects of device operation. By controlling where the space charges accumulate, the low recombination can be turned into an advantage. A high density of holes can directly benefit the emission intensity. By insertion of a hole blocking/electron injecting interlayer

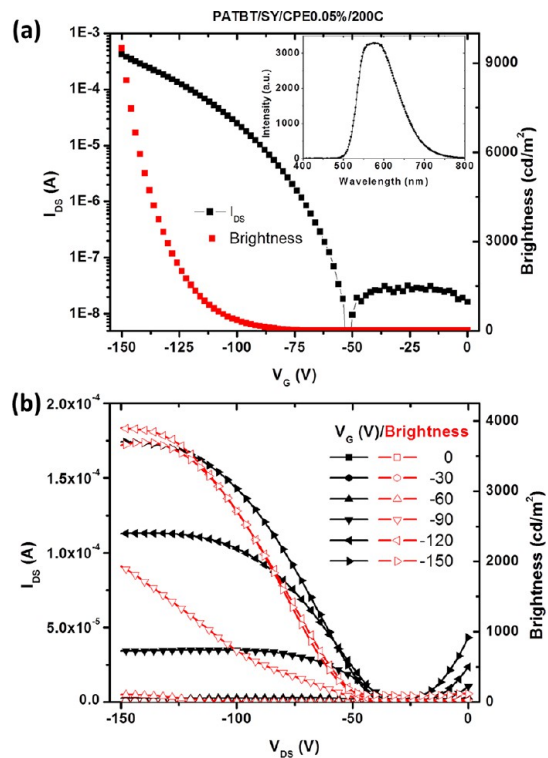


Figure 2. (a) Transfer and (b) output characteristics of bilayer LEFETs with correlated photoresponse. The inset in panel a shows the EL spectrum with peak at 570 nm.

between the luminescent polymer and the metal contacts, the hole density can be enhanced. We find that this high hole density functions to spatially extend

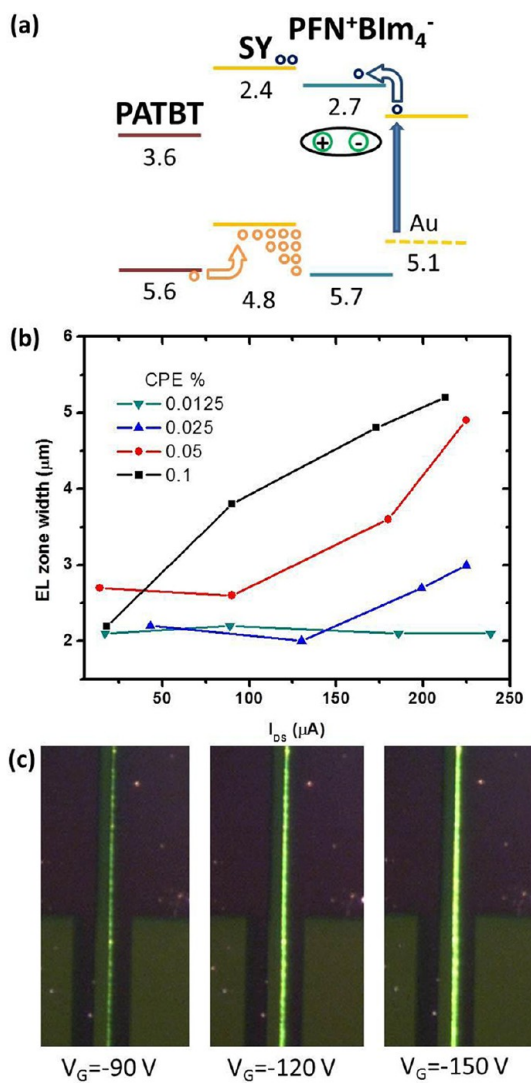
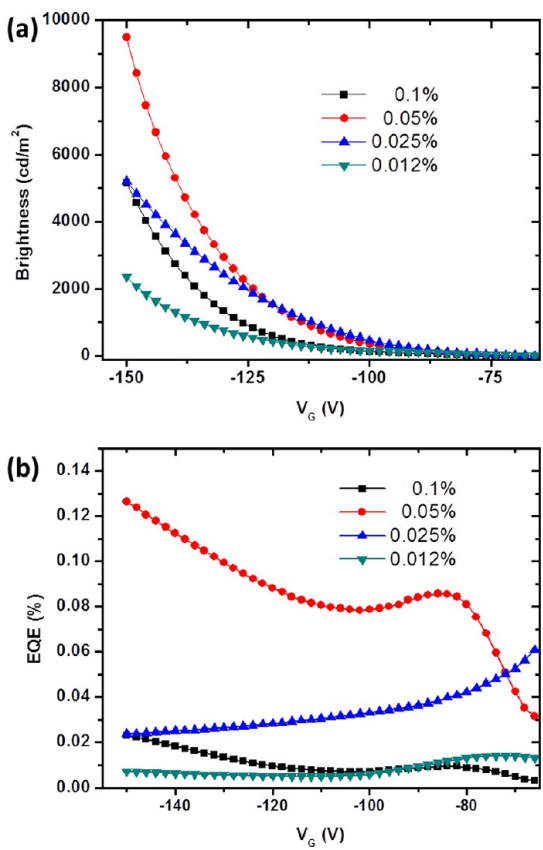


Figure 3. (a) Energy diagram of the different layers; (b) correlation between the EL zone width and current density obtained from output characteristic of  $V_G = -150$ ,  $-120$ ,  $-90$ , and  $-60$  V for devices with different CPE concentration; (c) operating photos obtained at different  $V_G$  of the device with 0.05 wt % CPE.

the recombination zone so that more photons are emitted, enabling the demonstration of high brightness ( $\sim 9500$  cd/m $^2$ ).

In this paper, we will first address the improved device parameters, such as brightness and electron injection from the textured substrate and CPE in Results and Discussion. We will then explore the core enhancement of the bilayer architecture, the morphological control of PATBT, including formation mechanism, optical and electronic anisotropy, and electrical characterization. It will be shown that the PATBT films with long-term order can improve both hole transport on the gate dielectric and the hole injection between PATBT and SY. The two aspects are discussed separately in the sections of Morphology of PATBT and Interfacial Improvement Driven by Thermal Annealing.



## RESULTS AND DISCUSSION

At high current densities, holes are the major carrier species. Because unbalanced charge transport between electrons and holes results in low emission efficiency, an interlayer between the metal contacts and the SY emitting layer that can inject electrons and block holes is required. The lowest unoccupied molecular orbital (LUMO) of the interlayer needs to match the LUMO of the SY for electron injection. Alternatively, the highest occupied molecular orbital (HOMO) of the interlayer should create an injection barrier to block the hole injection from the bottom PATBT. The conjugated polyelectrolyte (CPE) poly[9',9-bis[6'(N,N,N-trimethylammonium)hexyl]fluorene-alt-co-1,4-phenylene] with tetrakis(imidazoly)borate as the counterion ( $\text{PFN}^+\text{Blm}_4^-$ ) was proven to inject both electrons and holes at diluted concentration (0.02 wt %) and increased the turn-on threshold at high concentration ( $>0.2$  wt %).<sup>27,29,30</sup> Therefore, the interlayer shown in Figure 1 comprising dilute CPE can partially block holes without sacrificing current.

The LEFETs were fabricated on the structured substrates. Figure 2 panels a and b demonstrate the transfer and output characteristics of the LEFETs with 0.05 wt % CPE as well as the photoresponse correlated to the  $I-V$  profiles.  $V_G$  was swept from  $-150$  to  $0$  V and  $V_{DS}$  was biased at  $-150$  V in the transfer characteristic. For the output

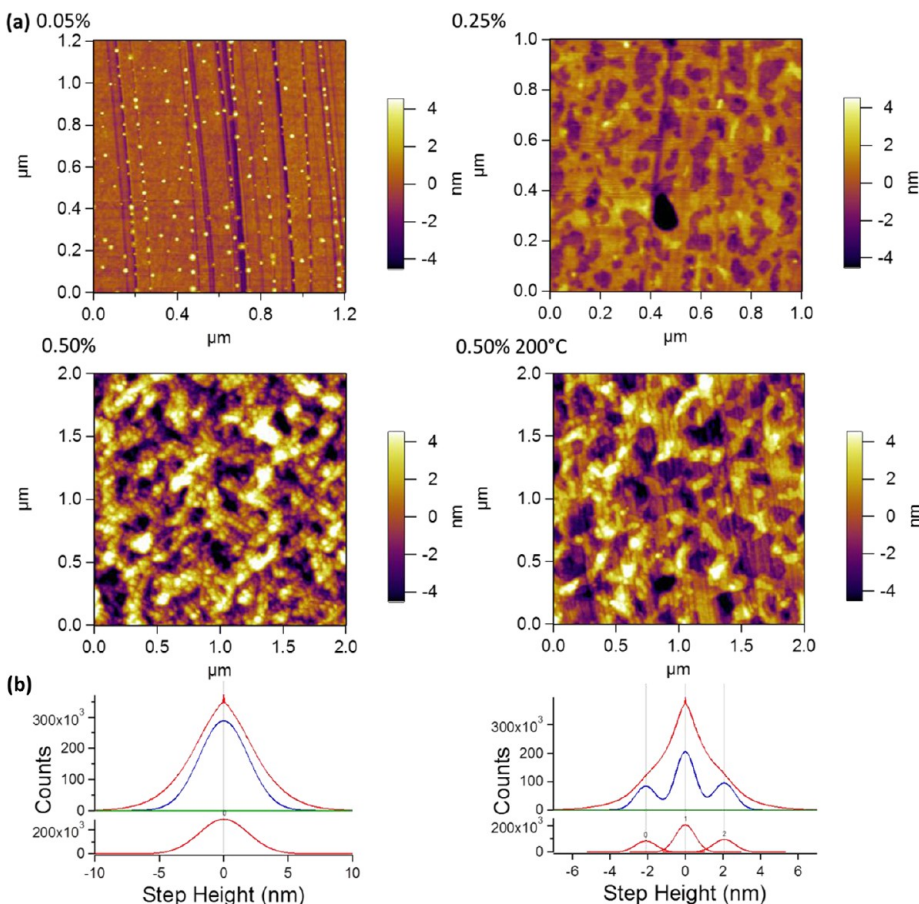


**Figure 5.** (a) AFM images of PATBT films. The films were prepared by spin coating various solution concentrations on the scratched substrates. (b) The statistics of the terrace step heights for 0.5 wt % films before and after annealing. The top graph of each shows the histogram of step heights (red) and the fitting which locates the dominant modes of the distribution (blue). The bottom shows the fitting separated into the individual Gaussian modes.

characteristic,  $V_{DS}$  was always swept from 0 to  $-150$  V while  $V_G$  was biased from 0 to  $-150$  V at  $-30$  V intervals. The average mobility extracted from the transfer characteristic between  $-100$  and  $-150$  V is  $0.30\text{ cm}^2/(\text{V s})$ . In the high-voltage operating regime,  $-140$  to  $-150$  V, the highest mobilities ( $0.47$  and  $0.52\text{ cm}^2/(\text{V s})$  in the output and transfer characteristics) were observed.

Brightness increases with current density up to a maximum of  $9493\text{ cd/m}^2$  at  $I_{DS} = 421\text{ }\mu\text{A}$ . Since the CPE film was spin-cast from a dilute solution, the resulting films were not continuous, and Au can inject holes into SY from the source electrode with no barrier as shown in the energy diagram of Figure 3a. Hence, the large threshold voltage ( $V_T$ ),  $-50$  V, results from the injection barrier created from the mismatched HOMO levels between SY/PATBT instead of PATBT/SY/CPE/Au. Once holes overcome the barrier at the SY/PATBT interface, PATBT can transport the high mobility holes and inject them into the SY. Then the CPE layer with deeper HOMO partially blocks holes awaiting the arrival of injected electrons with which to recombine.<sup>30</sup> Because holes are accumulating, their density increases and extends spatially as seen in Figure 3c. The EL zone widths and source–drain currents ( $I_{DS}$ ) shown in Figure 3b were obtained from the output

characteristics of  $V_G = -60, -90, -120$ , and  $-150$  V and  $V_{DS} = -150$  V. In Figure 3b, a clear positive correlation between the width of the luminescent zone and the current density is demonstrated; the wider the width of the emission zone, the higher the current density.

**Influence of CPE Concentration.** This effect is optimum for CPE solutions (in methanol) with concentrations higher than 0.0125 wt %. Therefore, concentrated CPE indeed blocks more holes and extends the width of the EL zone. In Figure 4 panels a and b, increasing CPE concentrations from 0.012, 0.025, to 0.05 wt % shows positive enhancement in both brightness and EQE. Therefore, the unbalanced transport with high hole density can perform better at high hole accumulation densities. Efficiency and brightness decrease after the CPE concentration increases to 0.1 wt % because too many holes are blocked by the injection barrier of the Au/CPE/SY interface at the source electrodes. At lower CPE concentration, brightness always shows higher values at large  $V_G$  ( $I_{DS}$ ). Outstanding brightness,  $>5000\text{ cd/m}^2$ , was achieved for CPE concentrations  $>0.012$  wt %. The emitted light could be seen by the bare eye in typical indoor lighting without using a microscope.

**Morphology of PATBT.** The nanostructure at the dielectric interface, produced by unidirectional lapping,

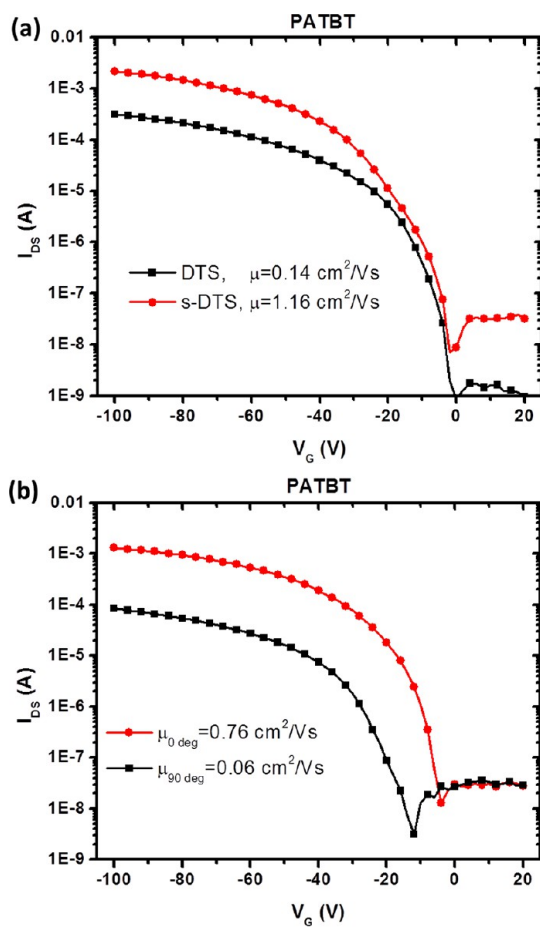


Figure 6. (a) FET performance obtained from the devices on the flat and scratched substrates; (b) the electronic anisotropy shown by mobility values between parallel (0 deg) and perpendicular (90 deg) to the grooves is consistent with the optical anisotropy in Supporting Information, Figure S2.

has a profound effect on the morphology and transport properties of the PATBT layer. It is instructive to examine the surface morphology as a function of the solution concentration (Figure 5a) on the scratched and passivated substrates. At a concentration of 0.05 wt %, the polymer forms small aggregates on the scratched substrate that cover only a small fraction of the substrate. The island-like aggregates have lateral dimensions of 30 to 35 nm and a height distribution between 5 and 7 nm. In addition, they are located almost exclusively along the scratches instead of dispersed randomly across the substrate, demonstrating the strong effect of the nanostructure on the self-assembly. The scratches themselves are typically less than a few nanometers deep, ~50 nm wide after passivation; however, they are difficult to characterize accurately as the dimensions are often comparable to the AFM tip. We postulate that the edges may template the 1D nucleation and growth of the polymer aggregates.

Increasing the polymer concentration to 0.25 wt % results in a nearly continuous thin film with terrace-like morphology. The shape of the terraces shows some anisotropy, elongated along the scratch direction, but this is difficult to quantify. A statistical analysis of the

terrace step heights (described in the Supporting Information and displayed in Figure 5b) shows the peak of the distribution to be 2.1 nm. This is in excellent agreement with specular X-ray diffraction (XRD) measurements (Supporting Information, Figure S1), which show the out-of-plane  $d$ -spacing to be 2.2 nm. This implies that each individual layer of the terraces is a well-defined molecular monolayer. Furthermore, the  $d$ -spacings from Figure S1 suggest that the polymer adopts an “edge-on” orientation where the backbones are parallel to the substrate and  $\pi$ -stacked in-plane, similarly to the well-known polymer PBT<sub>1,4</sub>T<sub>1,4</sub>T<sub>1,4</sub>,<sup>37</sup> which differs from this molecule only in the location of the solubilizing side-chains.

The highest transistor mobility is observed at a polymer concentration of 0.5 wt % without thermal annealing. Even though the PATBT films form more ordered polymer ribbons after thermal annealing, the mobility is slowly decreased from  $\sim 1 \text{ cm}^2/(\text{V s})$  at room temperature to  $\sim 0.5 \text{ cm}^2/(\text{V s})$  after 200 °C annealing (same as annealed bilayer LEFETs), implying ribbon boundaries may play a certain role in transport. As the film gets thicker, a loss of the terrace structure and any discernible orientational order from the substrate is observed. Instead, a nodule-like structure with a length scale similar to the polymer aggregates is demonstrated. The transistor performance on the scratched substrate is anisotropic and is significantly improved in the preferential transport direction as compared to the flat substrate. Parallel to the scratches, the mobility is a factor 4 higher on average with a maximum enhancement of factor 10 (Figure 6a). The ratio of the mobility parallel and perpendicular to the scratch direction varies from 3 to 10, indicating clear electronic anisotropy originally achieved by the as-cast films on the s-SAM. Measurement of the optical absorption on the as-cast film (Supporting Information, Figure S2) shows consistent anisotropy likely from material near the substrate. Thermal annealing at 200 °C changes the surface topography considerably; restoring an oriented phase at the top surface aligned with the scratched substrate. The optical anisotropy at 200 °C in Supporting Information, Figure S2 and the annealed topography in Figure 5a suggest the order at the structured substrate can propagate all the way to the top of the film upon thermal annealing, showing that the surface structures on the passivated dielectric can actually guide the polymer chains, forming long-term ordered ribbons.

**Interfacial Improvement Driven by Thermal Annealing.** A postannealing step after metal deposition causes a major improvement in the emission efficiency. Because PATBT is easily crystallized<sup>28</sup> it tends to become more ordered after thermal annealing (see XRD in Supporting Information, Figure S1). The crystallization process actually cures the partially mixed PATBT/SY from the second coating, and creates a better interface with SY. The enhancement on the optical output is obtained by the interface with less traps providing efficient hole injection. As shown

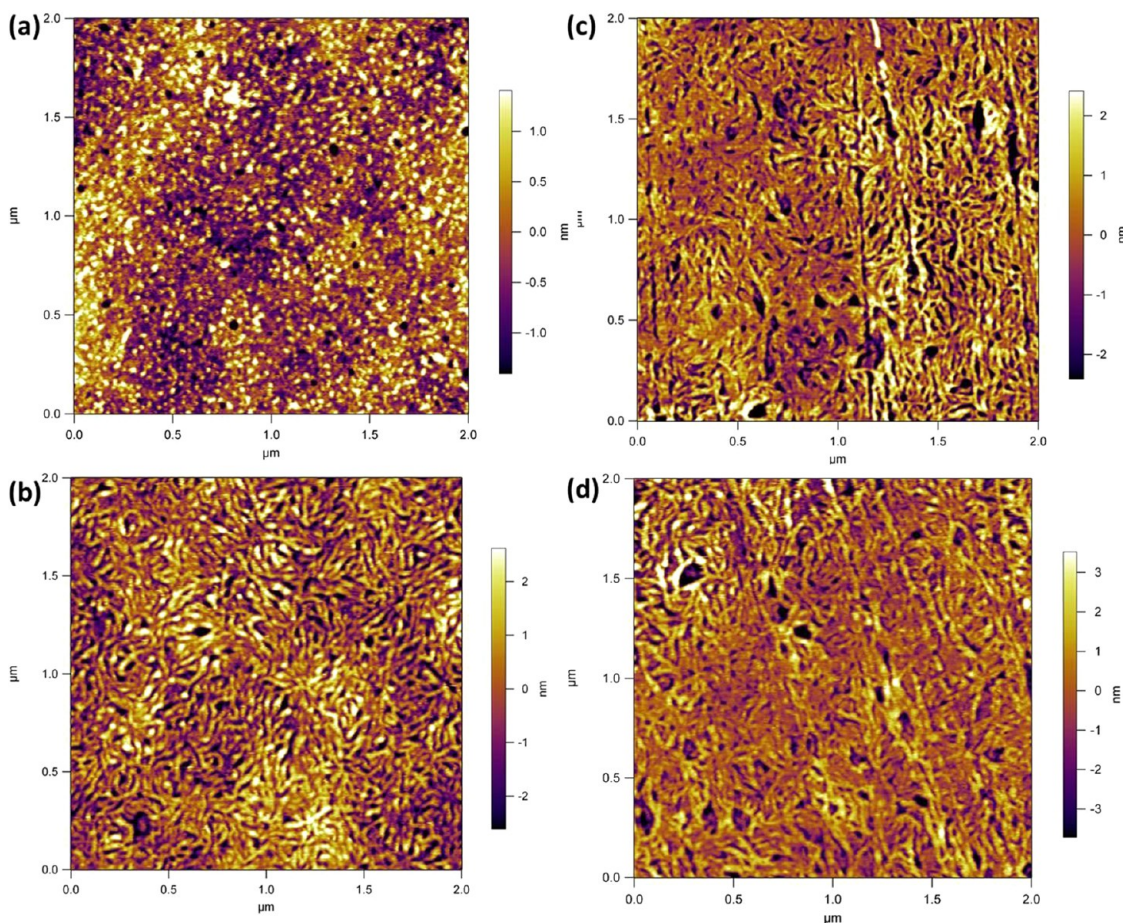


Figure 7. AFM images of the bottom PATBT layer on a flat substrate (a) as-cast and (b) after 200 °C annealing; (c) AFM images of the bottom PATBT layer on the structured substrate as-cast and (d) after annealing at 200 °C.

in Figure 7, after heating, PATBT formed fibers that are easily observed on the structured substrate. Figure 7a and Figure 7b are AFM images of the bottom PATBT films on flat  $\text{SiO}_2$  as-cast and annealed at 200 °C. Films were lifted from  $\text{SiO}_2$  substrates and transferred to another flat silicon substrate, bottom side up for topographic study. Figure 7c and Figure 7d show the morphology of the bottom PATBT as-cast and after 200 °C annealing on the structured  $\text{SiO}_2$ . Following introduction of grooves on the substrate, fibers grew after 100 °C soft baking on the structured substrates, whereas fibers were not observed on the nonstructured substrate. Wider bundles of PATBT on the structured dielectric can be observed in both Figure 7 panels c and d (compared with Figure 7b). Therefore, structured substrates can produce order leading to higher mobility and thereby benefit the strength of the light emission.

## CONCLUSIONS

The physical structure between the transistors and the passivated dielectric provides energetic preference on the surface, guides semiconducting polymers and forms ordered polymer fibers. Order in the PATBT raises carrier mobility and injects more holes into the luminescent SY layer. More holes accumulate because of the energy barrier introduced by the CPE at the drain electrode, therefore, holes distribute into a wider region in SY. While the current density increases, the recombination zone width simultaneously increases and emits more photons. To improve the efficiency, asymmetric contacts are foreseen as a next step. We expect that still higher brightness and efficiency should be achievable from bilayer LEFETs with asymmetric contacts.

## METHODS

**Transistor Fabrication.**  $\text{SiO}_2$  (200 nm) on heavily doped silicon substrate was structured with a lapping sheet with 100 nm diamond particles.<sup>39</sup> Silicon wafers were purchased from Silicon Quest and lapping sheets were obtained from Allied High Tech

Product Inc. Structured substrates were sonicated to clean the debris after scratching with the lapping sheet and then were passivated by decyl(trichlorosilane) (DTS) using the thermal immersion method, (80 °C for more than 20 min). DTS was purchased from Gelest Inc. PATBT purchased from Merck Chemicals Ltd. (EMD Chemicals) was dissolved in chlorobenzene at a

concentration of 0.5 wt %. The solutions must be heated over 80 °C before spin-casting at 5000 rpm for 40 s. The films were soft baked at 100 °C to dry and densify the films in order to resist the spin-casting of the second layer. A 0.6 wt % SY solution in toluene was then spin-cast at 1000 rpm for 50 s, and the bilayer films were baked at 120 °C for 10 min. To successfully fabricate a bilayer LEFET, high mobility and solvent resistance are critical considerations. The solvent resistance is essential to avoid interlayer mixing into the SY emitting layer. Therefore, a highly crystalline polymer that maintains excellent electronic properties after spin-casting the SY emitting layer is required. PATBT was therefore chosen as the bottom layer (closest to the gate dielectric). By using toluene (a very poor solvent for PATBT) for casting the SY layer, the crystallized PATBT remains stable on the dielectric interface. Devices were postannealed for 5 min at 200 °C before testing.

**Device Characterization.** All  $I-V$  data were collected by Keithley 4200. The emissive light was collected by a calibrated Hamamatsu photomultiplier. The external quantum efficiency (EQE) was calculated from the brightness, the drain current, and the emission spectrum of the device.<sup>1</sup> Postannealing and testing were all proceeded inside a glovebox with the oxygen level at less than 2 ppm oxygen. Specular XRD and grazing incidence XRD were performed on a Rigaku SmartLab diffraction system with a Cu  $K\alpha$  source, with specular measuring out-of-plane alignment and grazing incidence measuring in-plane alignment.

**Conflict of Interest:** The authors declare no competing financial interest.

**Acknowledgment.** Support for this research at UCSB was provided by the National Science Foundation (DMR 0856060). Support for the materials synthesis and characterization was provided by the National Science Foundation (DMR-1005546). Part of the material characterization was supported by Natural Science Foundation of China (No. 51010003, 50990065, and 21125419). We thank Dr. Andrea Gutacker and Dr. Jung Hwa Seo for providing the CPE materials. A portion of this work was performed in the UCSB nanofabrication facility, part of the NSF funded NNIN network. E.B.N. is a recipient of an Australian Research Council Future Fellowship (FT110100216).

**Supporting Information Available:** This material is available free of charge via the Internet at <http://pubs.acs.org>.

## REFERENCES AND NOTES

- Namdas, E. B.; Ledochowitsch, P.; Yuen, J. D.; Moses, D.; Heeger, A. J. High Performance Light Emitting Transistors. *Appl. Phys. Lett.* **2008**, *92*, 183304.
- Namdas, E. B.; Hsu, B. B. Y.; Yuen, J. D.; Samuel, I. D. W.; Heeger, A. J. Optoelectronic Gate Dielectrics for High Brightness and High-Efficiency Light-Emitting Transistors. *Adv. Mater.* **2011**, *23*, 2353–2356.
- Gwinn, M. C.; Kabra, D.; Roberts, M.; Brenner, T. J. K.; Wallukewitz, B. H.; McNeill, C. R.; Friend, R. H.; Sirringhaus, H. Highly Efficient Single-Layer Polymer Ambipolar Light-Emitting Field-Effect Transistors. *Adv. Mater.* **2012**, *24*, 2728–2734.
- Zaumseil, J.; Friend, R. H.; Sirringhaus, H. Spatial Control of the Recombination Zone in an Ambipolar Light-Emitting Organic Transistor. *Nat. Mater.* **2005**, *5*, 69–74.
- Muccini, M.; Nazionale, C. A Bright Future for Organic Field-Effect Transistors. *Nat. Mater.* **2006**, *605*–613.
- Zaumseil, J.; Donley, C. L.; Kim, J.-S.; Friend, R. H.; Sirringhaus, H. Efficient Top-Gate, Ambipolar, Light-Emitting Field-Effect Transistors Based on a Green-Light-Emitting Polyfluorene. *Adv. Mater.* **2006**, *18*, 2708–2712.
- Capelli, R.; Toffanin, S.; Generali, G.; Usta, H.; Facchetti, A.; Muccini, M. Light-Emitting Diodes. *Nat. Mater.* **2010**, *9*, 496–503.
- Gwinn, M. C.; Vaynzof, Y.; Banger, K. K.; Ho, P. K. H.; Friend, R. H.; Sirringhaus, H. Solution-Processed Zinc Oxide as High-Performance Air-Stable Electron Injector in Organic Ambipolar Light-Emitting Field-Effect Transistors. *Adv. Funct. Mater.* **2010**, *20*, 3457–3465.
- Swensen, J. S.; Soci, C.; Heeger, A. J. Light Emission from an Ambipolar Semiconducting Polymer Field-Effect Transistor. *Appl. Phys. Lett.* **2005**, *87*, 253511.
- Zaumseil, J.; McNeill, C. R.; Bird, M.; Smith, D. L.; Paul Ruden, P.; Roberts, M.; McKiernan, M. J.; Friend, R. H.; Sirringhaus, H. Quantum Efficiency of Ambipolar Light-Emitting Polymer Field-Effect Transistors. *J. Appl. Phys.* **2008**, *103*, 064517.
- Schidleja, M.; Melzer, C.; von Seggern, H. Electroluminescence from a Pentacene Based Ambipolar Organic Field-Effect Transistor. *Appl. Phys. Lett.* **2009**, *94*, 123307.
- Schidleja, M.; Melzer, C.; von Seggern, H. Investigation of Charge-Carrier Injection in Ambipolar Organic Light-Emitting Field-Effect Transistors. *Adv. Mater.* **2009**, *21*, 1172–1176.
- Bürgi, L.; Turbiez, M.; Pfeiffer, R.; Bienewald, F.; Kirner, H.-J.; Winnewisser, C. High-Mobility Ambipolar Near-Infrared Light-Emitting Polymer Field-Effect Transistors. *Adv. Mater.* **2008**, *20*, 2217–2224.
- Hepp, A.; Heil, H.; Weise, W.; Ahles, M.; Schmeichel, R.; von Seggern, H. Light-Emitting Field-Effect Transistor Based on a Tetracene Thin Film. *Phys. Rev. Lett.* **2003**, *91*, 1–4.
- Cicora, F.; Santato, C.; Dadvand, A.; Harnagea, C.; Pignolet, A.; Bellutti, P.; Xiang, Z.; Rosei, F.; Meng, H.; Perepichka, D. F. Environmentally Stable Light Emitting Field Effect Transistors Based on 2-(4-Pentylstyryl)tetraacene. *J. Mater. Chem.* **2008**, *18*, 158–161.
- Di, C. a.; Yu, G.; Liu, Y. Q.; Xu, X. J.; Wei, D. C.; Song, Y. B.; Sun, Y. M.; Wang, Y.; Zhu, D. B. Organic Light-Emitting Transistors Containing a Laterally Arranged Heterojunction. *Adv. Funct. Mater.* **2007**, *17*, 1567–1573.
- Suganuma, N.; Shimoji, N.; Oku, Y.; Okuyama, S.; Matsushige, K. Organic Light-Emitting Transistors with Split-Gate Structure and pn-Hetero-boundary Carrier Recombination Sites. *Org. Electron.* **2008**, *9*, 834–838.
- Nakanotani, H.; Saito, M.; Nakamura, H.; Adachi, C. Highly Balanced Ambipolar Mobilities with Intense Electroluminescence in Field-Effect Transistors Based on Organic Single Crystal Oligo(*p*-phenylenevinylene) Derivatives. *Appl. Phys. Lett.* **2009**, *95*, 033308.
- Gwinn, M. C.; Khodabakhsh, S.; Song, M. H.; Schweizer, H.; Giessen, H.; Sirringhaus, H. Integration of a Rib Waveguide Distributed Feedback Structure into a Light-Emitting Polymer Field-Effect Transistor. *Adv. Funct. Mater.* **2009**, *19*, 1360–1370.
- Mueller, T.; Kinoshita, M.; Steiner, M.; Perebeinos, V.; Bol, A. a.; Farmer, D. B.; Avouris, P. Efficient Narrow-Band Light Emission from a Single Carbon Nanotube p–n Diode. *Nat. Nanotechnol.* **2010**, *5*, 27–31.
- Namdas, E. B.; Samuel, I. D. W.; Shukla, D.; Meyer, D. M.; Sun, Y.; Hsu, B. B. Y.; Moses, D.; Heeger, A. J. Organic Light Emitting Complementary Inverters. *Appl. Phys. Lett.* **2010**, *96*, 043304.
- Maiorano, V.; Bramanti, a.; Carallo, S.; Cingolani, R.; Gigli, G. Organic Light Emitting Field Effect Transistors Based on an Ambipolar p–i–n Layered Structure. *Appl. Phys. Lett.* **2010**, *96*, 133305.
- Bisri, S. Z.; Takenobu, T.; Sawabe, K.; Tsuda, S.; Yomogida, Y.; Yamao, T.; Hotta, S.; Adachi, C.; Iwasa, Y. p–i–n Homojunction in Organic Light-Emitting Transistors. *Adv. Mater.* **2011**, *23*, 2753–2758.
- Gwinn, M. C.; Jakubka, F.; Gannott, F.; Sirringhaus, H.; Zaumseil, J. Enhanced Ambipolar Charge Injection with Semiconducting Polymer/Carbon Nanotube Thin Films for Light-Emitting Transistors. *ACS Nano* **2012**, *6*, 539–548.
- Hsu, B. B. Y.; Duan, C.; Namdas, E. B.; Gutacker, A.; Yuen, J. D.; Huang, F.; Cao, Y.; Bazan, G. C.; Samuel, I. D. W.; Heeger, A. J. Control of Efficiency, Brightness, and Recombination Zone in Light-Emitting Field Effect Transistors. *Adv. Mater.* **2012**, *24*, 1171–1175.
- Cavallini, M.; D'Angelo, P.; Criado, V. V.; Gentili, D.; Shehu, A.; Leonardi, F.; Milita, S.; Liscio, F.; Biscarini, F. Ambipolar Multi-stripe Organic Field-Effect Transistors. *Adv. Mater.* **2011**, *23*, 5091–5097.
- Seo, J. H.; Namdas, E. B.; Gutacker, A.; Heeger, A. J.; Bazan, G. C. Solution-Processed Organic Light-Emitting Transistors Incorporating Conjugated Polyelectrolytes. *Adv. Funct. Mater.* **2011**, *21*, 3667–3672.

28. McCulloch, I.; Heeney, M.; Chabiny, M. L.; DeLongchamp, D.; Kline, R. J.; Cölle, M.; Duffy, W.; Fischer, D.; Gundlach, D.; Hamadani, B.; *et al.* Semiconducting Thienothiophene Copolymers: Design, Synthesis, Morphology, and Performance in Thin-Film Organic Transistors. *Adv. Mater.* **2009**, *21*, 1091–1109.

29. Seo, J. H.; Namdas, E. B.; Gutacker, A.; Heeger, A. J.; Bazan, G. C. Conjugated Polyelectrolytes for Organic Light Emitting Transistors. *Appl. Phys. Lett.* **2010**, *97*, 043303.

30. Hoven, C. V.; Yang, R.; Garcia, A.; Crockett, V.; Heeger, A. J.; Bazan, G. C.; Nguyen, T.-Q. Electron Injection into Organic Semiconductor Devices from High Work Function Cathodes. *Proc. Natl. Acad. Sci. U.S.A.* **2008**, *105*, 12730–12735.

31. Moran-Mirabal, J. M.; Slinker, J. D.; DeFranco, J. a; Verbridge, S. S.; Ilic, R.; Flores-Torres, S.; Abruña, H.; Malliaras, G. G.; Craighead, H. G. Electrospun Light-Emitting Nanofibers. *Nano Lett.* **2007**, *7*, 458–463.

32. Campoy-Quiles, M.; Ishii, Y.; Sakai, H.; Murata, H. Highly Polarized Luminescence from Aligned Conjugated Polymer Electrospun Nanofibers. *Appl. Phys. Lett.* **2008**, *92*, 213305.

33. Pagliara, S.; Camposeo, A.; Cingolani, R.; Pisignano, D. Hierarchical Assembly of Light-Emitting Polymer Nanofibers in Helical Morphologies. *Appl. Phys. Lett.* **2009**, *95*, 263301.

34. Pagliara, S.; Camposeo, A.; Polini, A.; Cingolani, R.; Pisignano, D. Electrospun Light-Emitting Nanofibers as Excitation Source in Microfluidic Devices. *Lab Chip* **2009**, *9*, 2851–2586.

35. Das, A. J.; Lafargue, C.; Lebental, M.; Zyss, J.; Narayan, K. S. Three-Dimensional Microlasers Based on Polymer Fibers Fabricated by Electrospinning. *Appl. Phys. Lett.* **2011**, *99*, 263303.

36. Vohra, V.; Giovanella, U.; Tubino, R.; Murata, H.; Botta, C. Electroluminescence from Conjugated Polymer Electrospun Nanofibers in Solution Processable Organic Light-Emitting Diodes. *ACS Nano* **2011**, *5*, 5572–5578.

37. Ribbons, N.; DeLongchamp, D. M.; Kline, R. J.; Jung, Y.; Germack, D. S.; Lin, E. K.; Moad, A. J.; Richter, L. J.; Toney, M. F.; Heeney, M.; *et al.* Controlling the Orientation of Terraced. *ACS Nano* **2009**, 780–787.

38. O'Connor, B.; Kline, R. J.; Conrad, B. R.; Richter, L. J.; Gundlach, D.; Toney, M. F.; DeLongchamp, D. M. Anisotropic Structure and Charge Transport in Highly Strain-Aligned Regioregular Poly(3-hexylthiophene). *Adv. Funct. Mater.* **2011**, *21*, 3697–3705.

39. Tseng, Hsin-Rong; Ying, Lei; Hsu, Ben B. Y.; Perez, Louis; Takacs, C. J.; Bazan, G. C.; Heeger, A. J. High Mobility Field Effect Transistors Based on Macroscopically Oriented Regioregular Copolymers. *Nano Lett.* **2012**, *12*, 6353–6357.

40. Jimison, L. H.; Toney, M. F.; McCulloch, I.; Heeney, M.; Salleo, A. Charge-Transport Anisotropy Due to Grain Boundaries in Directionally Crystallized Thin Films of Regioregular Poly(3-hexylthiophene). *Adv. Mater.* **2009**, *21*, 1568–1572.